Ultrasonics Sonochemistry 77 (2021) 105693

Contents lists available at ScienceDirect

Ultrasonics Sonochemistry

journal homepage: www.elsevier.com/locate/ultson

Effects of ultrasonic treatment and homogenization on physicochemical properties of okara dietary fibers for 3D printing cookies

Yaowen Liu [a,*,1], Shengkui Yi [a,1], Tingting Ye [a], Ying Leng [a], Md Alomgir Hossen [a], Dur E. Sameen [a], Jianwu Dai [b], Suqing Li [a], Wen Qin [a,*]

[a] College of Food Science, Sichuan Agricultural University, Yaan 625014, China
[b] College of Mechanical and Electrical Engineering, Sichuan Agricultural University, Yaan 625014, China

ARTICLE INFO

Keywords:
Okara
Modified
Dietary fiber
3D printing
Cookie

ABSTRACT

This paper presents a means to modify the attributes of okara fiber using ultrasonic and high-speed shearing treatment. The results of scanning electron microscopy and differential scanning calorimetry reveal that the modified okara fiber demonstrates small particle size and high thermal stability. When the 500 W–15,000 rpm combination is used for okara-fiber treatment, the latter exhibits excellent swelling (SC) as well as water- and oil-holding capacities. When 6% of modified okara fiber is added to the dough, the resulting cookies demonstrate the best printing performance. Subsequently, the printing parameters can be optimized to obtain the best filling rate of 30%. The corresponding nozzle diameter and printing speed equal 0.8 mm and 50 mm/s, respectively. Finally, the 3D-printed cookies containing okara fiber are compared against those commonly available in the market via sensory evaluation. As observed, the 3D-printed cookies were more acceptable to people. Therefore, the addition of the okara dietary fiber to the cookie dough not only improves the okara utilization rate but also increases the dietary-fiber content in the cookie, thereby alleviating the occurrence of obesity in modern society.

1. Introduction

Okara (soybean residue) is a byproduct obtained during the production of soy products such as tofu, soymilk, yuba, soy protein isolate. Soybeans (1 kg) are used in the production of soy products, which produce approximately 1.1–1.2 kg of wet okara [1]. However, dry okara contains various nutrients including 50%–60% dietary fiber (DF), 20%–30% crude protein, 10%–12% lipids, and other nutrients such as isoflavones, minerals, and saponins [2]. Therefore, okara is a high-quality source of DF. Based on its solubility, DF can be divided into soluble dietary fiber (SDF) containing pectin, xanthan gum, and dextran and insoluble dietary fiber (IDF) containing cellulose, hemicellulose, and lignin [3].

Since IDF has adverse effects on various aspects of food quality such as functionality and sensory perception, it is generally not incorporated into food [4]. Therefore, it is particularly important to modify the IDF. Common modification methods that are currently used include physical and chemical methods, enzymatic reactions, and microbial fermentation. By modifying the IDF in okara, its related performance can be enhanced. It has been reported that several methods including steam explosion, cavitation jet, high-pressure homogenization, K. marxianus fermentation, and carbohydrase mixture can modify DF. Studies have shown that the application of steam explosion can increase the content of SDF in okara [5]. Alkali treatment homogenization can not only change the physicochemical properties of insoluble soybean fiber, but can also enhance its emulsifying properties [6]. It has been reported that a cavitation jet can be used to improve the DF function of okara [7]. High-pressure homogenization is beneficial in increasing the content of proteins and SDF in okara [1]. Wang et al. found that by combining the fermentation of K. marxianus with β-glucosidase, the IDF in okara can be modified more effectively [8]. Ullah et al. were able to narrow the particle size of the IDF in okara to the nanometer range through wet milling [9]. It has been reported that carbohydrase mixture treatment can increase the content of the SDF and sugar in the okara, and reduce the content of the IDF [10].

In various food-processing industries, ultrasound has been considered an efficient, green technology. In recent years, ultrasound has increasingly been used in combination with other technologies in the

* Corresponding authors.
E-mail addresses: lyw@my.swjtu.edu.cn (Y. Liu), qinwen@sicau.edu.cn (W. Qin).
[1] These authors contributed equally to the work.

https://doi.org/10.1016/j.ultsonch.2021.105693
Received 28 April 2021; Received in revised form 30 June 2021; Accepted 22 July 2021
Available online 25 July 2021

food industry [11]. It has been reported that high-intensity ultrasound can destroy the crystal structure of the okara fiber and enhance its water-holding capacity (WHC) [12]. Zhang et al. extracted SDF from a papaya peel using an ultrasound-assisted alkali extraction method, and the results showed that the SDF has high thermal stability, WHC, and oil-holding capacity (OHC) [13]. Some studies have shown that SDF can be extracted from flaxseed gum, and compared three extraction methods: enzymatic, ultrasound-enzymatic, and alkaline methods. The SDF content extracted using the ultrasonic-enzymatic method is the highest [14]. Compared to thermal, enzymatic, and chemical treatment, ultrasonic treatment is simpler to implement and has higher extraction efficiency. It can enhance the water-holding, oil-holding, swelling, and rheological properties of DF to some extent [15]. In addition, high-speed shear homogenization also has a wide range of applications in the extraction and modification of DF. It has been pointed out in the literature that the okara fiber modified through high-speed shearing can decompose the constituent cells at the cellular level, and the okara fiber has better solubility [16]. Pectin-rich DF was prepared from a citrus peel by the combination of alkaline hydrogen peroxide and high-speed homogenization. Compared to commercial fibers, the DF of the composite-treated pectin had excellent hydration and large surface area [17]. The residual DF in sausage casings was characterized by the combination of enzymatic hydrolysis and high-speed homogenization, which indicates that the residual cellulose casings are a good source of DF [18]. Different extraction methods were used to characterize the SDF obtained from coffee peels. The results showed that the shear-assisted enzymatic treatment could obtain the highest SDF yield and glucose absorption capacity [19]. Based on the above discussion, ultrasound and high-speed shear were combined to modify the IDF in okara, and the modified okara fiber was added to cookie dough. Finally, cookies with different shapes and rich DF were printed using 3D printing technology.

Cookies, a type of baked food, are favored by consumers owing to their unique taste. However, most recipes for cookies include high sugar, high fat, and low DF content. With the improvement in people's living standards, long-term consumption of such high-sugar and high-fat foods can easily make them obese, exposing them to the risk of diabetes. Therefore, it is very important to develop cookies with DF. It has been reported that adding fresh okara to improver starch, soy flour, and hydroxypropyl methylcellulose can enhance the fiber and nutritional value of cookies [20]. The incorporation of biovalorised okara can further enhance the texture of cookies, and enhance the SDF and antioxidant properties of okara [21]. Cross-linked wheat starch can be used to develop cookies with high fiber and low glycemic index [22]. Compared to the traditional cookie making method, the nutrition customization of 3D food printing technology has attracted the attention of consumers.

With the continuous development in 3D printing technology, 3D printing is also facing new challenges in the food field. For 3D printed food raw materials, we can perform targeted nutritional fortification of food raw materials according to the requirements of specific groups of people. Furthermore, we can meet the nutritional needs of the consumers through dietary adjustments [23]. To establish a 3D-printed food system, such as 3D printing dough, the printability of the food raw materials is mainly based on the rheological properties of the ink. Common cookie dough is viscoelastic and fluid, and is formed by mixing wheat flour and water. This property is called the rheology of the dough and is closely related to the quality of 3D-printed cookies. Sun et al. combined low-field nuclear magnetic resonance and partial least squares regression to evaluate the rheological properties of microwave-treated 3D printed cookie dough [24]. The results suggested that the partial least squares regression model could accurately evaluate the rheological properties of cookie dough [25]. The antioxidant extracted from Arthrospira platensis was encapsulated in alginate microbeads and then added to the 3D-printed cookies to provide antioxidant functionality to the cookies. The study reported that by changing the recipe of the cookie dough, the printability and post-processing of the 3D-printed cookie dough were affected. Changes in various ingredients can also affect the physical properties of the 3D-printed cookie dough [23]. In addition, preheating has a certain correlation with the internal structure, printability, and dimensional stability of the 3D-printed cookie dough [26]. Nevertheless, 3D-printed cookies with DF functionality have not been reported in the existing studies.

In this study, we developed 3D-printed cookie with DF functionality. First, the IDF was extracted from okara and physically modified through ultrasound and high-speed shearing. Second, the modified okara was characterized through SEM, XRD, FT-IR spectra, differential scanning calorimetry (DSC), swelling power, WHC, and OHC. The optimized conditions were screened out, and then the physically modified okara was added to the cookie dough. The printability and texture of the cookie dough containing DF were determined through the rheological properties and texture profile analysis (TPA) of the dough. Finally, the printing parameters were optimized and the 3D printed cookies containing DF were compared against those available on the market based on sensory evaluation.

2. Materials and methods

2.1. Materials

Okara used in this study was purchased from Dazhou Luyexiang Food Co., Ltd. (Dazhou, China). Wheat flour, butter, powdered sugar, and milk were purchased from a local supermarket in Ya'an City, Sichuan Province, China. Sodium hydroxide (NaOH) and hydrochloric acid (HCl) were purchased from Chengdu Haoboyou Reagent Co., Ltd. (Chengdu, China). Unless otherwise stated, all other chemical reagents and solvents were of analytical grade and purchased from Chengdu Kelon Reagent Co., Ltd. (Chengdu, China).

2.2. Preparation of okara IDF

We made appropriate modifications to the method proposed by Ullah et al [27]. for the extraction of IDF from okara. First, okara was defatted with petroleum ether. Subsequently, defatted okara was added to 1 mol/L NaOH at a weight ratio of 1:15 and stirred at a constant speed of 800 rpm at 50 °C for 3.5 h. After stirring, the sample was filtered with gauze and the okara residue was washed to neutral with distilled water. In addition, neutral okara was added to 1 mol/L HCl with a weight ratio of 1:15 and stirred at a constant speed of 800 rpm at 50 °C for 3.5 h. Then, the okara residue was again washed to neutral with distilled water. Finally, the residue was dried in an oven at 55 °C for 48 h to obtain the IDF sample.

2.3. Ultrasound treatment

The dried okara IDF was coarsely ground with a pulverizer (LD-300, Changsha Hongjing Machinery Equipment Co., Ltd., China) for 30 s and screened with a 120-mesh sieve. Further, 5 g of the sifted okara powder and 100 ml of distilled water were thoroughly mixed using a magnetic stirrer (DJ1C, Changzhou Guohua Electric Co., Ltd., China) at 500 rpm for 45 min to obtain okara powder suspension. Herein, the ultrasound treatment based on the method suggested by Fan et al [12]. was slightly modified. Briefly, an ultrasonic processor (KS-T, Shanghai Keqi Instrument Equipment Co., Ltd., China) with a high-grade titanium alloy probe was used to process the prepared suspension. At room temperature, the titanium alloy probe was immersed in the center of the suspension at a depth of approximately 2 cm, and its output power was set to 400, 500, and 600 W for the ultrasonic treatment of the suspension for 30 min (3 s : 2 s work/rest cycles). The samples were vacuum-freeze dried at − 50 °C until they reached a constant weight and stored in a desiccator at room temperature (25 °C) for further investigations.

2.4. High-speed homogenization

The modification effect of high-speed homogenization on okara IDF was tested, for which 100 ml of okara IDF suspension was loaded in a 250 ml beaker and homogenized by a high-speed shear homogenizer (AD500S-H, Changzhou Jintan Liangyou Instrument Co., Ltd., China). The shear speed was set to 5,000, 10,000, and 15,000 rpm, and the shear time equaled 10 min. The samples were vacuum-freeze dried at − 50 °C until they reached a constant weight, and were stored in a desiccator at room temperature (25 °C) for further investigations.

2.5. Combined processing of ultrasound treatment and high-speed homogenization

To study the modification effect of the combined processing of ultrasonic treatment and high-speed homogenization on okara IDF, the okara IDF first underwent an ultrasonic treatment, according to Section 2.3. Then, high-speed homogenization treatment was performed according to Section 2.4. The samples were vacuum-freeze dried at − 50 °C until they reached a constant weight, and were stored in a desiccator at room temperature (25 °C) for further investigations. Based on the power output and shear speed in the combined processing, the samples were distributed in nine groups: 400 W-5000 rpm, 500 W- 5,000 rpm, 600 W-5,000 rpm, 400 W-10,000 rpm, 500 W-10,000 rpm, 600 W-10,000 rpm, 400 W-15,000 rpm, 500 W-15,000 rpm, and 600 W-15,000 rpm.

2.6. Preparation of cookie dough

To determine the best dough formulation for 3D printing, we slightly modified the crafting recipe proportions of Kim et al [28]. First, powdered sugar was added to softened butter and beaten with a whisk until it was smooth. Second, wheat flour was added to the mixture in small quantities multiple times. The mixture was subsequently stirred at a constant speed for 2 min while milk was slowly introduced to the system. Finally, the modified okara IDF was added to the mixture system until the system reached the desired viscosity, to obtain uniform cookie dough. The dough recipe is presented in Table 1.

2.7. Scanning electron microscopy

The lyophilized okara IDF powder was attached to a specimen holder with a double-sided tape, and then the samples were sputter-coated with a layer of gold (thickness = 5 nm). The microstructures of the okara IDF were observed through SEM (Fei Quanta 200, Netherlands) at a voltage of 10 kV.

2.8. X-ray diffraction

The crystalline structure of the okara IDF was observed using an X-ray diffractometer (MPX3, MAC Science, Japan) at 40 kV and 30 mA. The diffraction angle (2θ) was set in the 5°–70° range, and the scanning rate was 2°/min.

Table 1
In the cookie dough formulations, wheat flour was partially replaced by modified okara IDF.

Ingredients	Modified okara IDF in cookie dough (g/100 g)				
	Control	2%	4%	6%	8%
Wheat flour	35	33	31	29	27
Butter	25	25	25	25	25
Powdered sugar	22	22	22	22	22
Milk	18	18	18	18	18
Modified okara IDF	0	2	4	6	8
Total	100	100	100	100	100

2.9. Fourier-transform infrared spectroscopy (FT-IR)

For the okara IDF, the change in molecular structure was analyzed using an infrared spectrometer (Nicolet iS1S0, Thermo Nicolet Inc., USA). The IDF and KBr (1:100, w/w) were fully mixed and then pressed into a disk for infrared analysis. The wavenumbers of FT-IR spectra were in the range of 650–4000 cm^{-1}, and each sample was scanned 32 times.

2.10. Differential scanning calorimetry

The thermal stability of okara fiber was studied using a differential scanning calorimeter (Q200 V24.2 Build 107, USA). A sample of approximately 5 mg was taken and sealed in an aluminum pan; subsequently, the parameters values were set for heating the sample from 10 °C to 300 °C at a heating rate of 10 °C min^{-1}.

2.11. Color analysis

Color change in the okara fibers was measured using a colorimeter (CR-400, Konica Minolta, Tokyo, Japan). A white standard plate was used as the background, and the CIE L* (lightness, color transition from dark to light), a* (red-green intensity), and b* (yellow-blue intensity) color space parameters were obtained. Whiteness index (WI) and total color difference (ΔE*) were calculated as follows:

$$WI = 100 - \sqrt{(100 - L)^2 + a^2 + b^2} \quad (1)$$

$$\Delta E* = \sqrt{(\Delta L*)^2 + (\Delta a*)^2 + (\Delta b*)^2} \quad (2)$$

where ΔL*, Δa*, and Δb* denote the differences between the color values of the standard color plate and okara fiber samples.

2.12. Particle size determination

Okara IDF (1:10 (v/v)) was diluted in deionized water and then placed on a vortex shaker for uniform mixing. At 25 °C, the particle size of IDF dispersion was analyzed using a Malvin laser particle size analyzer (Rise-2006, Runzhi Technology Co., Ltd., Jinan, China), and the refractive index of the solution was set to 1.333.

2.13. Determination of zeta potential (ζ)

At 25 °C, the zeta potential of the okara IDF suspension was measured using a dynamic light scattering instrument (Rise-2006, Runzhi Technology Co., Ltd., Jinan, China). Before testing, the IDF suspension was diluted with deionized water and subsequently ultrasonicated for 30 min.

2.14. Swelling capacity, water-holding capacity, and oil-holding capacity

The method described by Wang et al. was slightly modified [16]. First, 1 g (M0) of okara IDF was diluted in 75 ml (V0) of deionized water and magnetically stirred for 24 h. Then, the volume of the suspension (V1) was recorded, and the suspension was centrifuged at a rotational speed of 6000 rpm for 10 min. The supernatant was removed, and the weight of the wet fiber (M1) was recorded. The SC and WHC of the wet fiber were calculated as follows:

$$SC(mL/g) = \frac{V1 - V0}{M0} \quad (3)$$

$$WHC(g/g) = \frac{M1 - M0}{M0} \quad (4)$$

The OHC of okara fiber was slightly modified according to the method of Hua et al [29]. First, 1 g (M0) of okara fiber was mixed with 20 ml of soybean oil under magnetic stirring for 24 h. Then, the

suspension was centrifuged at 3000 rpm for 20 min, its supernatant was poured out, and the weight of the remaining okara fiber (M1) was recorded. The OHC was calculated as follows:

$$OHC(\mathrm{g}/100g) = \frac{M1 - M0}{M0} \quad (5)$$

2.15. Rheological properties

The rheological properties of the cookie dough were measured using a rheometer (Discovery HR-2, TA Instruments, USA). In addition, the parameters of the rheometer were as follows: the diameter of the parallel plate, gap width, and temperature equaled 40 mm, 1050 μm, and 25 °C, respectively. The viscoelasticity of the cookie dough was measured in the linear viscoelastic region using the dynamic oscillation frequency sweep mode. The dynamic oscillation frequencies in the range of 0.1–100 rad/s were analyzed at a strain of 0.4%, and the storage modulus (G'), loss modulus (G ‘‘), and loss angle tangent (tanδ) were recorded [30]. To stabilize the apparent viscosity, the viscosity and shear stress of each sample were used as a function of shear rate (0.1–100 s^{-1}). Finally, the data were fitted to the Herschel–Bulkley model, as follows:

$$\tau = \tau_0 + k\gamma^n \quad (6)$$

Here, τ denotes the shear stress (Pa), τ_0 denotes the yield stress (Pa), K denotes the consistency index (Pa·sn), γ denotes the shear rate, and n denotes the flow behavior index.

2.16. Texture profile analysis

The texture profile of the 3D-printed products were analyzed using the method proposed by Liu et al [31]. The hardness, adhesiveness, springiness, and gumminess of the 3D-printed product were tested using a texture analyzer (Stable Micro System Ltd., Leicestershire, UK) with probe P/0.5.

2.17. Three-dimensional printing process

The three-dimensional printing apparatus composed an X-Y-Z positioning mechanism, screw pneumatic linkage extrusion, and feeding systems. The printing was performed without any supporting structure. The movement and positioning in the 3D printing process were controlled through custom-made JAVA programs and microcontrollers based on computers, which play an important role in the entire printing process. During the printing process, the relative positions on the X, Y, and Z axes were controlled by the Cura 15.04.6 (UltimakerBV, Netherlands) software, which guided the nozzle to move along a specific path. The entire printing process was performed at room temperature (25 °C). The 3D printer used in this study, which combines a screw and pneumatic extrusion system, is more tolerant of ink compared to other traditional 3D printers.

Printing parameters were optimized to evaluate their influence on the geometry of the extrudate. For different printing speeds and nozzle diameters, cylinders were extruded at the same extrusion rate to optimize the printing parameters. Finally, different filling rates of the samples were explored.

2.18. Sensory evaluation of 3D printed cookies

In this study, the team responsible for performing the sensory evaluation comprised 30 panelists with good sensory discriminative ability. All participants volunteered to perform this evaluation and become part of this study. Six sensory parameters of the 3D-printed cookies, namely their appearance, color, crispiness, taste, flavor, and overall quality were evaluated on a five-point hedonic rating scale (1 = very poor, 2 = poor, 3 = good, 4 = very good, 5 = excellent) [32]. In addition, the 3D-printed DF cookies were compared with their fiber-rich, fiber-free, and ordinary cookie counterparts purchased from a local supermarket. The cookies were delivered in coded containers in random order. All panelists were provided with mineral water to clean their oral cavities between successive sample tastings.

2.19. Statistical analysis

All data in the experiment were expressed as mean ± standard deviation (SD). One-way analysis of variance (ANOVA) was performed with SPSS 22.0 statistical analysis system. $P < 0.05$ was considered statistically significant.

3. Results and discussion

3.1. Characterization of okara fibers

3.1.1. SEM

Fig. 1 shows the microstructure of okara IDF modified using different physical modification methods. As shown in Fig. 1a1 and a2, the okara fiber in the control group was in a lump with a smooth surface and a tight texture, indicating that lipids, crude proteins, and other components in okara can be removed through acid–base digestion. This is consistent with previous reports [9]. The okara IDF in the control group exhibited a smooth and compact structure, which may be because of the molecular interactions making the okara fiber surface smooth and unbroken [12]. Fig. 1b1 and b2 show the microstructure of okara fiber under ultrasonic treatment. It can be seen that the okara fiber decomposed from a lumpy structure into a flaky structure and stacked together during the ultrasonic treatment. This is because ultrasound deforms cell tissue and disintegrates the cellulose packing of the cell wall [12]. In addition, the ultrasonic treatment destroys the crosslinking between polysaccharide molecules [13]. If the ultrasonic power is significantly high, the okara fiber will be destroyed at the cellular level. Therefore, any change in the surface of the okara fiber structure changes causes its particle size to reduce. Moreover, the functionality of the okara fiber also changes with the change in its structure. The microstructure of the okara fiber under high-speed shear treatment is shown in Fig. 1c1 and c2. Under the action of high-speed shearing, the okara fiber sheared into layers of flakes. Moreover, its surface also exhibits several cracks, which are attributed to the fact that high-speed shearing has strong mechanical shearing, hydraulic friction, tearing, and other effects [17]. After high-speed shearing, the parenchyma of the okara fiber was deformed, hourglass cells were broken, and hourglass cells and corneum were detached. In other words, high-speed shearing may effectively disintegrate the constituent cell layers at the cellular level [16]. Fig. 1d1 and d2 show the microstructure of okara fiber under ultrasound treatment–high-speed shearing combined processing (UT-HSH). The okara fibers treated by UT-HSH have honeycomb-like parenchyma with loose internal structure and more cracks on the surface. This may be because the internal structure and surface area of the okara fiber were significantly damaged under the action of the physical factors—ultrasound and shear. Through SEM, we confirmed the effect of the UT-HSH treatment on the modification of the morphology and microstructure of the okara fiber. Moreover, the change in the microstructure of the okara fiber further determines its physical and chemical properties, such as water-holding and swelling capacities.

3.1.2. XRD

As shown in Fig. 2a, the XRD patterns were used to evaluate the effects of different physical modification methods on the crystal structure of okara fibers. Fibers are mainly composed of cellulose, hemicellulose, and lignin. Nevertheless, owing to the presence of cellulose, the okara fibers are composed of crystalline and amorphous (non-crystalline) regions, in which the non-crystalline region mainly contains hemicellulose and lignin [33]. It can be seen that all the modified okara

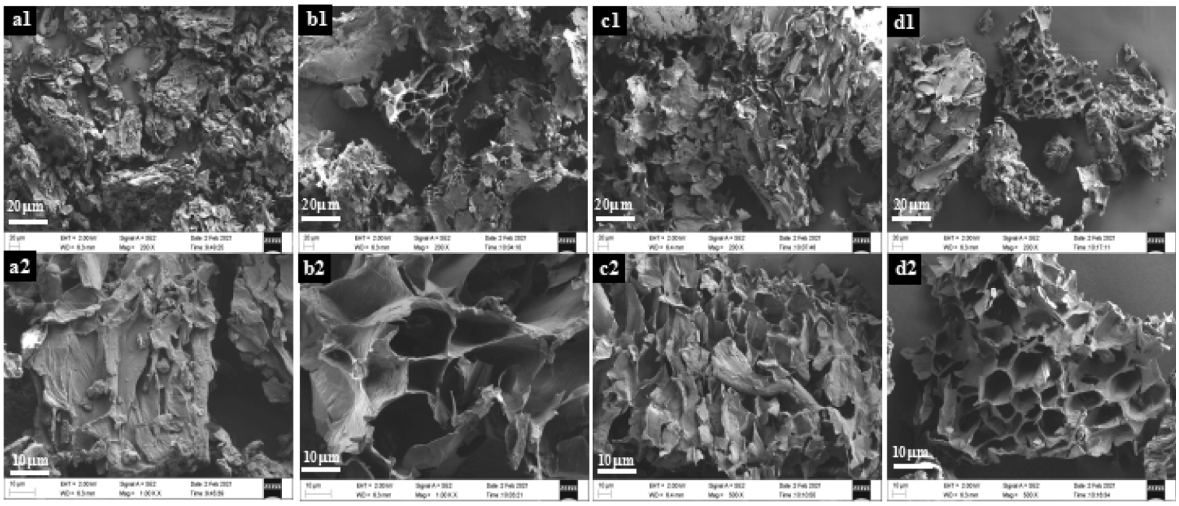

Fig. 1. SEM visualizations of okara fiber treated using different methods, SEM photos of control group, UT, HSH, and UT-HSH obtained at (a1–d1) 20 μm and (a2–d2) 10 μm, respectively.

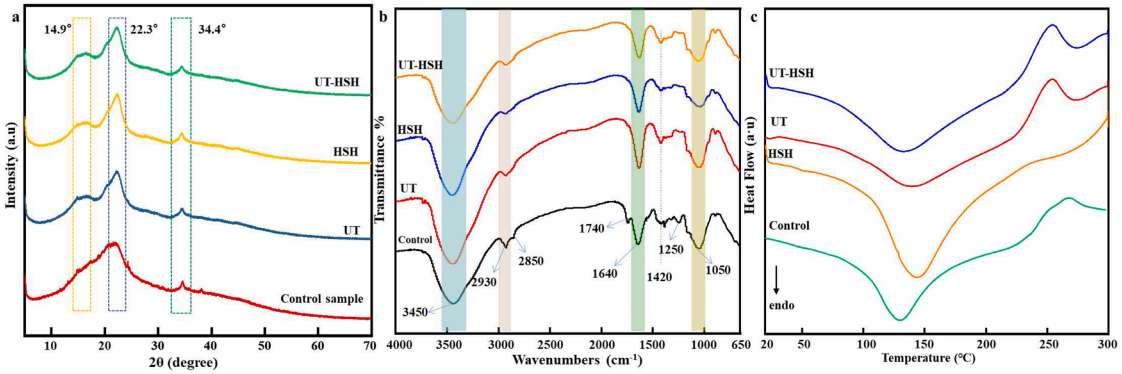

Fig. 2. (a) XRD, (b) FT-IR and (c) DSC curves obtained for okara fiber treated using different methods.

fibers show a similar trend. The okara fiber showed prominent characteristic diffraction peaks at approximately 22.3° with minor 2θ peaks at 14.9° and 34.4°. This indicates the existence of cellulose crystal regions and a cellulose I-type crystal structure [34,35]. In this form of cellulose, both the crystalline and amorphous (non-crystalline regions) regions coexist. After being treated using different physical modification methods, both the regions decreased to different degrees. This indicates that the crystalline and amorphous regions of the okara fibers could be decomposed through physical modification [16]. Correspondingly, the particle size of the modified IDF was also reduced. This may be due to the destruction of the crystalline regions of the okara fibers during the physical modification process to obtain smaller crystals. This result is similar to that reported by Ullah et al [9]. There is no obvious difference in the position and width of the 2θ peaks of the physically modified okara fiber. This indicates that although the crystalline region in the okara fiber has been converted to small crystals, its ordered structure has not been destroyed [3].

3.1.3. FT-IR spectra

Fig. 2b shows the FT-IR spectra of the okara fiber samples from 4000 to 650 cm^{-1}, which were used to analyze the molecular groups and chemical bonds of IDF. It can be seen that all samples exhibit similar FT-IR spectra. For all samples, the wide absorption band in the range of 3250–3650 cm^{-1} is attributed to O–H stretching, mainly due to the presence of polysaccharides, particularly cellulose and hemicellulose, in okara [36]. The weak absorption bands at 2930 cm^{-1} and 2850 cm^{-1} are attributed to the asymmetric and symmetric C–H vibrations of polysaccharide methylene, respectively [12]. Compared to the control sample, some characteristic peaks gradually disappeared. The absorption bands at 1740 cm^{-1} and 1250 cm^{-1} disappeared due to the C = O stretching of the aldehyde/ester group and the stretching of the aromatic skeletal [37]. Aldehydes, esters, carboxyl groups, and other components are mainly present in hemicellulose, lignin, and partial proteins. When the okara fibers were treated with ultrasound or high-speed shearing, hemicellulose, lignin, and protein were destroyed, thereby resulting in the disappearance of the characteristic peaks. The absorption bands at 1640 cm^{-1} and 1420 cm^{-1} are attributed to the stretching of aromatic benzene carboxyl groups C = O and C–O in lignin [37]. Moreover, the peak at 1050 cm^{-1} is attributed to the stretching vibrations of a C–O bond, in particular, the glycosidic bond (C–O–C) in cellulose [3]. By this time, IDF can be decomposed into oligosaccharides. In summary, ultrasound or high-speed shearing can break the hydrogen bonds between cellulose and hemicellulose, and the UT-HSH combined treatment produces strong destructive force to break the chemical bonds in DF, which decreases the particle size and increases the hydrophilicity of the modified fiber.

3.2. DSC

Fig. 2c shows the DSC thermogram of okara fiber in the temperature range of 20–300 °C. This thermogram was used to analyze the thermal stability of the modified okara fiber. It can be clearly seen that all samples exhibit an endothermic and exothermic peak. The temperature range of the first absorption peak is 130–150 °C, and the largest peak is

at approximately 143 °C, which is attributed to the evaporation of bound water in DF [13]. The exothermic peak displayed in the curve corresponds to the thermal decomposition, oxidative decomposition, and elimination of volatile products of DF. The decomposition of polysaccharides was caused by the destruction of the glycosidic bonds [38]. The exothermic peak appears at approximately 250 °C, which can be attributed to the decomposition of hemicellulose (pectin) [13]. In addition, it can be seen from Fig. 2c that the heat flow strength of both the control group and okara fiber after high-speed shearing is high, which indicates that their thermal stability is relatively low. However, the okara fiber treated by ultrasound has lower heat flow intensity and higher thermal stability. This is because the ultrasonic treatment increases the crystallinity of cellulose in the okara fiber, which requires a higher temperature to decompose. Moreover, the ultrasonic treatment reduces the content of hemicellulose and lignin in the okara fiber and increases the hydroxyl content of cellulose, thereby improving their thermal stability [39]. Therefore, it can be seen that the thermal stability of the UT-HSH-treated okara fiber is not as high as that of the ultrasound-treated okara fiber.

3.2.1. Color

In the food industry, color is one of the important parameters of food ingredients and affects the acceptability of food products by consumers. In addition, changes in food color help us to distinguish changes in the physical and chemical properties of raw food materials. The CIE values and WI of okara IDFs under ultrasonic, high-speed shear, and UT-HSH treatment conditions are listed in Table 2. It can be seen that the color parameters of the control and treated samples are significantly different ($p < 0.05$). The okara fibers of the control group have a block-like structure, as shown in Fig. 1a; the layers are not completely separated from each other, and there is a lot of dark space. Therefore, the okara fibers are yellowish brown with low lightness (small L value). After the okara IDFs were treated by ultrasound or high-speed shearing, the lightness of the okara powder significantly improved (L value increased), which is attributed to the destruction of the okara fiber, resulting in the change in its surface structure and reduced area of the dark space (Fig. 1 b and c). When the okara fibers were treated by the combination of ultrasound and high-speed shear, their lightness (L value) and WI both changed significantly ($p < 0.05$), because with the increase in the ultrasonic power and rotation speed, the okara fibers were destroyed at the cellular level. This resulted in the separation of hourglass cells and stratum corneum, thus exhibiting small particle size, high brightness, and smooth and delicate powder surface. This is similar to the results reported by Ullah et al [9]. However, the 500 W-10,000 rpm okara fibers exhibited higher a*(+redness) and b*(+yellowness) values and a relatively low WI. This may be due to the occurrence of the Maillard reaction during the treatment [40].

Table 2
Color parameters of okara Insoluble Dietary Fiber (IDF) under different processing methods, such as lightness (L*), redess/greenness (a*), yellowness/blueness (b*), total color differences (ΔE) and whiteness index (WI).

Treatment	L*	a*	b*	ΔE	WI
Control	84.45 ± 0.35^{f}	0.88 ± 0.04^{e}	15.79 ± 0.82^{a}	23.43 ± 0.85^{a}	77.82 ± 0.76^{i}
400w	86.07 ± 0.53^{e}	0.41 ± 0.05 ^{g}	8.45 ± 0.42^{f}	15.89 ± 0.40^{gh}	82.98 ± 0.54^{gh}
500w	86.41 ± 0.44^{e}	0.6 ± 0.14^{f}	10.51 ± 0.30^{d}	17.96 ± 0.29 ^{cd}	83.54 ± 0.47^{fgh}
600w	87.48 ± 0.32^{bcd}	0.75 ± 0.10^{ef}	10.63 ± 0.14^{d}	17.85 ± 0.18 ^{cd}	84.56 ± 0.57^{cde}
5000r	84.70 ± 0.51^{f}	0.82 ± 0.13^{e}	15.91 ± 0.18^{a}	23.49 ± 0.28^{a}	82.86 ± 0.40 ^{h}
10000r	86.91 ± 0.69^{cde}	0.42 ± 0.14 ^{g}	9.42 ± 0.77^{e}	16.75 ± 0.72^{efg}	83.85 ± 0.65^{efg}
15000r	87.57 ± 0.56^{bcd}	0.08 ± 0.09 ^{h}	8.12 ± 1.13^{f}	15.34 ± 1.05 ^{h}	84.75 ± 0.53^{cde}
400w-5000r	86.95 ± 0.44^{cde}	1.27 ± 0.04^{abcd}	10.35 ± 0.04^{d}	16.38 ± 0.59 ^{fg}	83.51 ± 0.53^{fgh}
400w-10000r	87.69 ± 0.49^{bc}	1.35 ± 0.08^{ab}	11.57 ± 0.11^{bc}	17.57 ± 0.36^{de}	84.23 ± 0.36^{def}
400w-15000r	87.93 ± 0.26^{bc}	1.26 ± 0.09^{abcd}	11.29 ± 0.08 ^{cd}	17.28 ± 0.46^{def}	84.95 ± 0.56^{bcd}
500w-5000r	86.57 ± 0.58^{de}	1.28 ± 0.17^{abc}	12.00 ± 0.83^{bc}	19.31 ± 0.83^{b}	84.73 ± 0.43^{cde}
500w-10000r	86.95 ± 0.53^{cde}	1.39 ± 0.05^{a}	12.38 ± 0.68^{b}	19.63 ± 0.69^{b}	85.17 ± 0.54^{abcd}
500w-15000r	88.5 ± 0.4^{b}	1.10 ± 0.08^{d}	11.61 ± 0.38^{bc}	18.73 ± 0.40^{bc}	85.41 ± 0.55^{abc}
600w-5000r	88.38 ± 0.71^{b}	1.21 ± 0.03^{bcd}	10.32 ± 0.05^{d}	18.23 ± 0.35 ^{cd}	85.38 ± 0.45^{abc}
600w-10000r	89.53 ± 0.55^{a}	1.25 ± 0.03^{abcd}	10.57 ± 0.11^{d}	18.76 ± 0.46^{bc}	85.75 ± 0.53^{ab}
600w-15000r	90.34 ± 0.46^{a}	1.17 ± 0.08 ^{cd}	10.36 ± 0.02^{d}	17.29 ± 0.40^{def}	85.99 ± 0.47^{a}

3.2.2. Particle size determination

Fig. 3a shows the particle size distribution and average particle size of okara fiber under various treatments. The particle size distribution of the okara fiber in the control group is mainly in the range of 80.08–370.88 μm, and its average particle size is 123.97 μm. In addition, it can be seen that the average particle size of the okara fibers treated by ultrasound and high-speed shearing is lower than that of the control sample, and the okara fiber after high-speed shearing treatment exhibits a higher volume fraction. This can be attributed to the cavitation effect of ultrasound, which deforms the okara fiber cell tissue and destroys its surface structure, thereby resulting in a decrease in the particle size [41]. High-speed shearing can effectively disintegrate the constituent cell layers of the okara fiber [16]; hence, the fiber particle size is smaller and the volume fraction is higher. The average particle size of the okara fiber decreased to 49.41, 36.39, and 42.74 μm, when different ultrasonic power outputs and shearing speeds were combined to treat the okara fibers. It can be clearly seen that with the increase in ultrasonic power, the average particle size gradually decreases. However, when the ultrasonic power is increased to 600 W combined with high-speed shearing, the average particle size of the okara fiber increases to 42.74 μm. This is because high-power ultrasound can destroy the crosslinking between the polysaccharide molecules in okara fiber, and combined with high-speed shearing, results in smaller okara fiber particles. It has been reported in the literature that when the particle size is less than a certain value, due to van der Waals and electrostatic interactions, the smaller fiber particles will regroup together [42]. In addition, Ullah et al. have reached a similar conclusion that the particle size of okara IDF slightly changes after grinding for 6 h [9].

3.2.3. Zeta potential (ζ) determination

Zeta potential (ζ) was used to show that the stability of a suspension is a measurement of the interfacial potential between the aqueous and stationary phases, which plays a crucial role in the shelf life of a product [9,27]. Fig. 3b shows the results of zeta potential of okara fiber under different treatments. The zeta potential (negative value) of the control sample was 9.82 mv and those (negative value) of the suspension after ultrasonic and high-speed shearing treatment increased to 17.7 mv and 25.23 mv, respectively. The results show that the increase in the surface negative charge is beneficial in improving the stability of the okara suspension. This is due to the breaking of bonds between cellulose and other polysaccharides in the okara fiber under ultrasonic cavitation and mechanical shearing, thereby resulting in smaller particle size and larger specific surface area. Larger surface area leads to the exposure of more free polar groups and release of charged soluble fibers, thereby forming a strong electrostatic attraction and exhibiting a higher zeta potential [17]. The zeta potential (negative value) of the suspension treated by UT-HSH was 27.13 mv, which showed the best dispersion stability.

3.2.4. Swelling capacity, water-holding capacity, and oil-holding capacity

The WHC and OHC of the okara fiber are extremely important in food

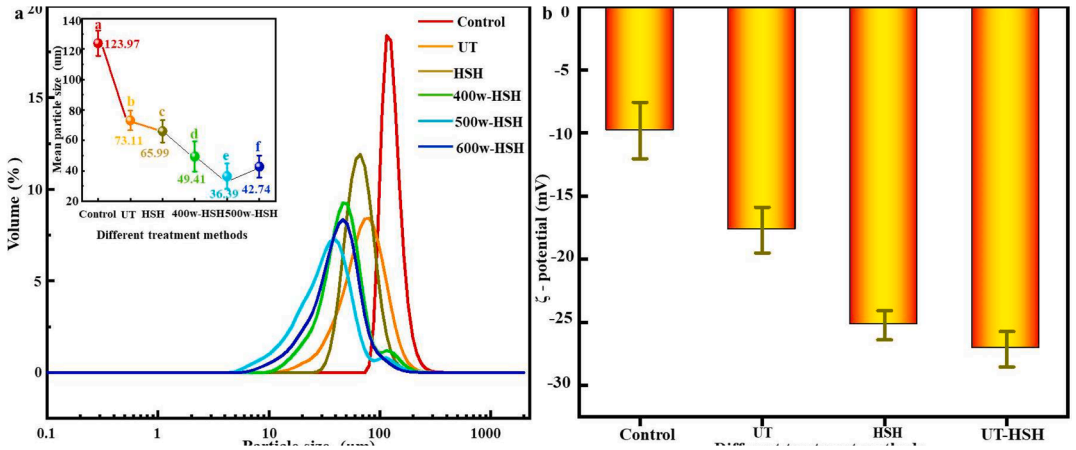

Fig. 3. Effect of different treatment methods on particle-size distribution, (a) average particle size of okara fiber, and (b) stability of the okara suspension.

applications. A higher WHC indicates that it can lock more moisture in the food and reduce food shrinkage caused by dehydration. In addition, the hydrophilic group and reticular structure of the DF in the okara are the basis of WHC formation. The OHC is related to the fiber particle size distribution, charge density, and polysaccharide composition of okara [17]. A higher OHC indicates greater stability of high-fat foods (such as cookies), as well as improved sensory properties and longer shelf life. The SC, WHC, and OHC of the okara fiber depend on the change in its internal structure. Fig. 4 shows the trends concerning the SC, WHC, and OHC of okara fibers treated with different methods. The SC and WHC of

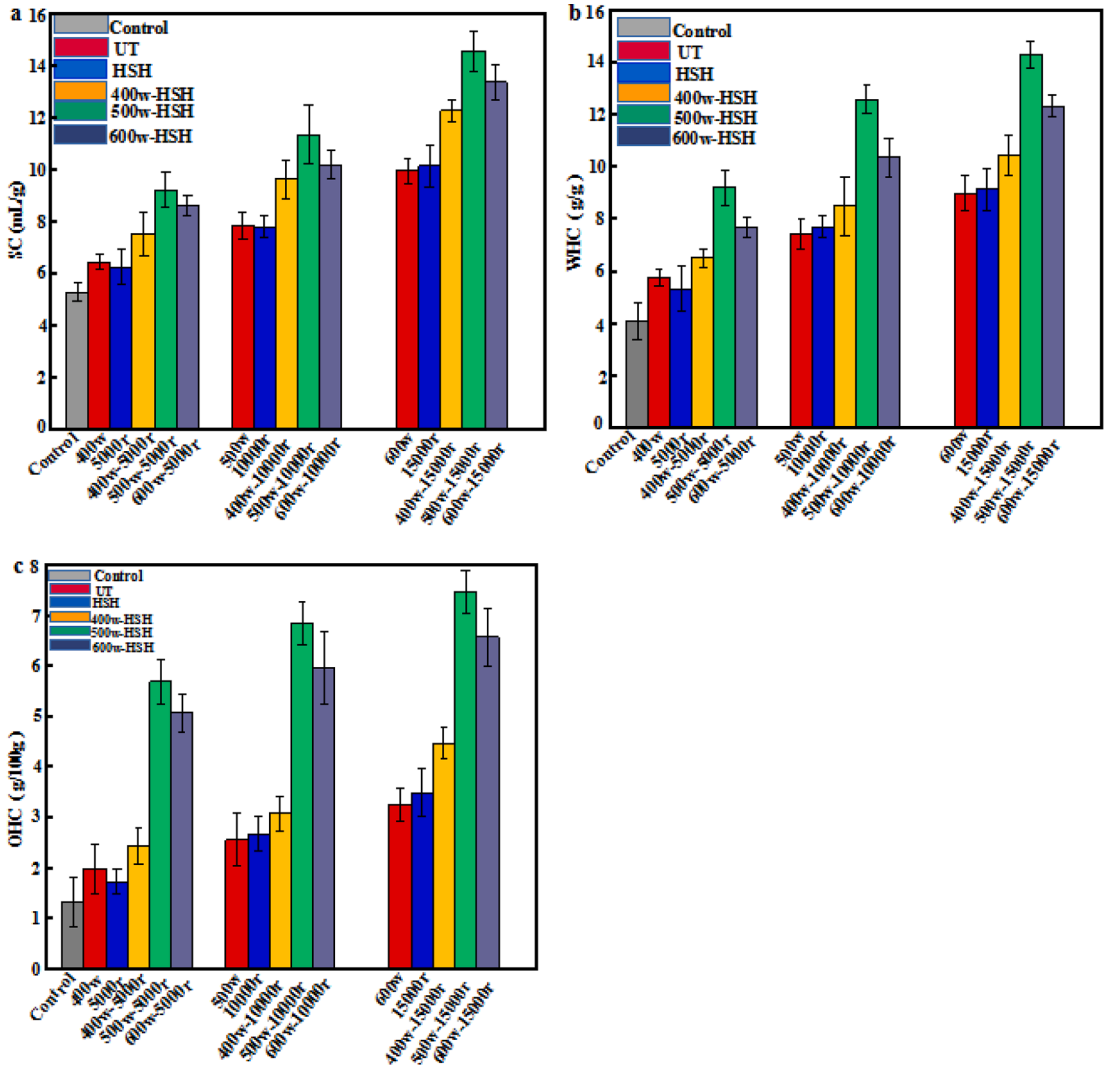

Fig. 4. Effect of different treatment methods on physical and chemical properties of okara fiber, (a) swelling capacity, (b) water-holding capacity, and (c) oil-holding capacity.

the okara fiber increase with the increasing power of ultrasound or speed of shearing. In the UT-HSH-treated okara fiber, the SC and WHC increased significantly due to the exposure of its hydrophilic groups and the changes in the internal structure of the okara fiber [16]. When the suspension was treated with 500 W-HSH, the particle size of the okara fiber further reduced (Fig. 3). Therefore, owing to smaller particle size, larger specific surface area, and higher WHC, the SC increases [27]. However, when the suspension was treated with 600 W-HSH, both the SC and WHC decreased significantly, which was attributed to the destruction of the porous structure of the okara fiber. Its internal structure was loose, and there were more surface cracks (Fig. 1), leading to decreased moisture capture ability of the okara fiber matrix [29]. The combination of UT-HSH produces a strong destructive force, thereby destroying the hydrogen bonds within cellulose and causing some characteristic peaks to drop or disappear. This also causes adsorption of water in the bean dregs matrix to become difficult. When 500 W-15,000 rpm was used, its OHC increased to the maximum value, which could be due to the relatively loose texture of the treated okara fiber. In addition, it can be observed that the maximum SC, WHC, and OHC can be obtained when the suspension is treated with 500 W-15,000 rpm. Therefore, we added the okara fiber obtained after the 500 W-15,000 rpm treatment to the cookie dough for further analysis.

3.3. Printability test of cookie dough

3.3.1. Rheological properties

The rheological properties of food, such as viscosity, storage modulus, and loss modulus, are crucial parameters that are used to evaluate the printability of the materials [43]. Viscosity refers to the internal friction between the molecules in the food inks to resist their flow [44]. The apparent viscosity of the inks at high shearing rates should be low enough to ensure that the inks can be extruded from a smaller nozzle, but high enough to support a layer-by-layer deposited structure [45]. Fig. 5a shows that the apparent viscosity of the cookie dough decreases with the increasing shear rate. This indicates that the cookie dough is a pseudoplastic fluid that exhibits shear thinning, which facilitates the extrusion of ink from nozzles with smaller diameters. In addition, the increase in the proportion of okara fiber results in an increase in its apparent viscosity. This can be attributed to the increase in the SC and WHC with the increasing okara fiber content, which is conducive to maintaining the extrusion shape [46]. The Herschel–Bulkley model is widely used for pseudoplastic materials for fitting the flow curve [46], and the parameter values are reported in Table 3. It can be clearly seen that all n values are<1, which indicates that the cookie dough is a non-Newtonian fluid. When the okara fiber addition increase from 0 to 8%, the behavior of the cookie dough gradually changes from Newtonian to the shear thinning type (i.e., n decrease from 0.53 to 0.27 and τ_0 increased from 415.58 Pa to 5870.84 Pa). This indicates that a cookie dough with higher okara fiber concentration exhibits high mechanical strength and better shape retention ability [47]. K indicates that the viscosity of cookie dough increased from 47.25 to 894.45 Pa·s^n, which implies that the cookie dough with 8% okara fiber content showed poor extrudability, i.e., it is not easy to extrude it from the nozzle tip during printing. G' is a measure of elastic solid-like behavior, and it also reflects the mechanical strength of the

Table 3
Herschel-Bulkley model parameters for the flow curve of cookie dough with different concentrations of okara fiber.

Okara Fiber Addition	τ_0(Pa)	K(Pa·s^n)	n	R^2
0	415.58	47.25	0.53	0.984
2%	446.33	176.68	0.45	0.981
4%	1438.69	225.74	0.43	0.985
6%	3752.49	473.75	0.36	0.972
8%	5870.84	894.45	0.27	0.923

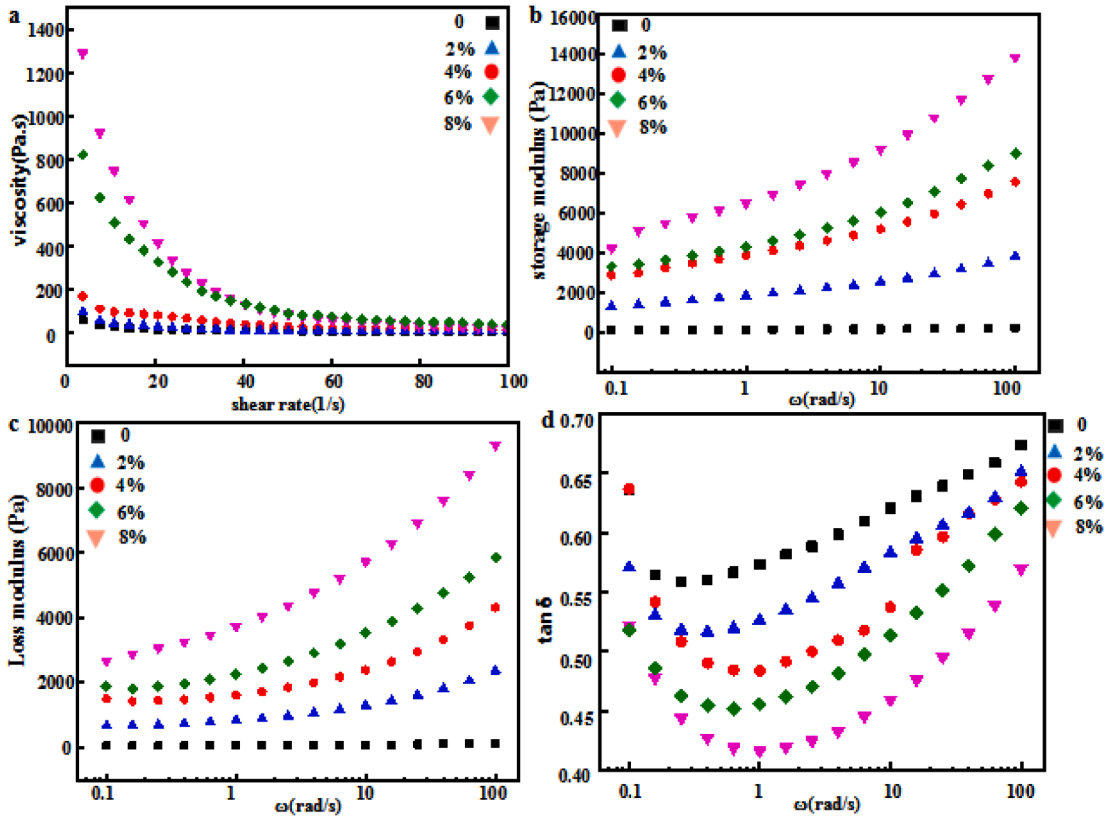

Fig. 5. Rheological behavior (a) apparent viscosity, (b) storage modulus (G'), (c) loss modulus (G"), and (d) tan δ—of cookie dough containing different okara-fiber concentrations.

ink. G'' is the viscous response, which is the ratio of stress to strain under dynamic oscillation frequency analysis. The loss-angle tangent (tan δ) of $G''/G'>1$ indicates a predominantly viscous characteristic, and a value smaller than 1 indicates a predominantly elastic property [43]. However, both G' and τ_0 can be used to pre-treat the mechanical strength of the cookie dough. In general, the higher the values of G' and τ_0, the more compressed the ink is, and the part used for printing exhibits good self-supporting properties [47]. The viscoelastic properties of all the samples are shown in Fig. 5b and c. It can be seen that in the linear viscoelastic region, G' is always higher than G", indicating that the inks had the potential to form an elastic gel or a gel-like structure. With the increasing okara fiber content, both G' and G" increased significantly, which indicates the presence of strong mechanical strength inside the cookie dough. This may be due to the increase in the SC and WHC in the okara fiber, which formed a dense 3D network structure. As shown in Fig. 5d, the tan δ values of all the cookie doughs are<1, indicating that the cookie doughs exhibit more solid behavior and poor fluidity. As can be observed, tan δ first decreased and then increased with the increasing frequency. In addition, the tan δ value of the cookie dough with the okara fiber was lower than that of the control group, indicating that the WHC of the okara fiber can increase the crosslinking degree of the molecules in the cookie dough.

3.3.2. Texture profile analysis

Fig. 6 shows the results of the TPA of the cookie dough containing the okara fiber. As the content of the okara fiber increased from 0 to 8%, the hardness and gumminess of cookie dough increased significantly ($P < 0.05$). When the content of the okara fiber increased to 6%, the cookie dough exhibited the highest adhesiveness. As the content of the okara fiber increases continuously, the adhesiveness tends to decrease. This may be because the addition of the okara fiber increases the WHC of the cookie dough, which results in an interaction between the lipid and protein in the dough. However, it can be seen that when the content of the okara fiber was increased to 6% and 8%, no significant difference in the springiness ($P \geq 0.05$) of the cookie dough was observed. The hardness and springiness of the cookie dough showed a contrary trend with the addition of the okara fiber. The cookie dough exhibited maximum hardness and minimum springiness when 8% of the okara fiber content was added, and the dough did not easily extrudate from the nozzle aperture, which is similar to that observed in the rheological analysis above. Moreover, the addition of the okara fibers to the cookie dough during heating may induce the formation of covalent and disulfide bonds between the protein molecules, thereby forming a compact internal network that provides a high support force against the external deformation [48]. Therefore, the above results indicate that using 6% okara fiber cookie dough can be better extruded from the nozzle.

3.4. 3D printing process

3.4.1. Optimization of internal filling ratio

The stability of the 3D-printed food model designed by CAD requires the mechanical properties of an internal support structure to be maintained [49]. Therefore, in the experimental study, a cylinder model was used to optimize the 3D printing parameters, and the impact of different filling rates (a1 = 10%, a2 = 30%, a3 = 50%, a4 = 70%) on the print quality were tested (Fig. 7a). As shown in Fig. 7b, the decreasing internal filling rate will weaken the support strength of the whole food and destroy its surface structure (Fig. 7b1). However, with the increasing internal filling rate, the accumulation of the internal cookie dough will further affect the printing precision (Fig. 7b3 and b4) [50]. When the filling rate of the cylinder is 30%, its interior presents a self-supporting cross support structure, which exhibits better stability and printing precision (Fig. 7b2). In addition, it was reported that the 3D shapes of chocolate were designed with different supporting structures, such as

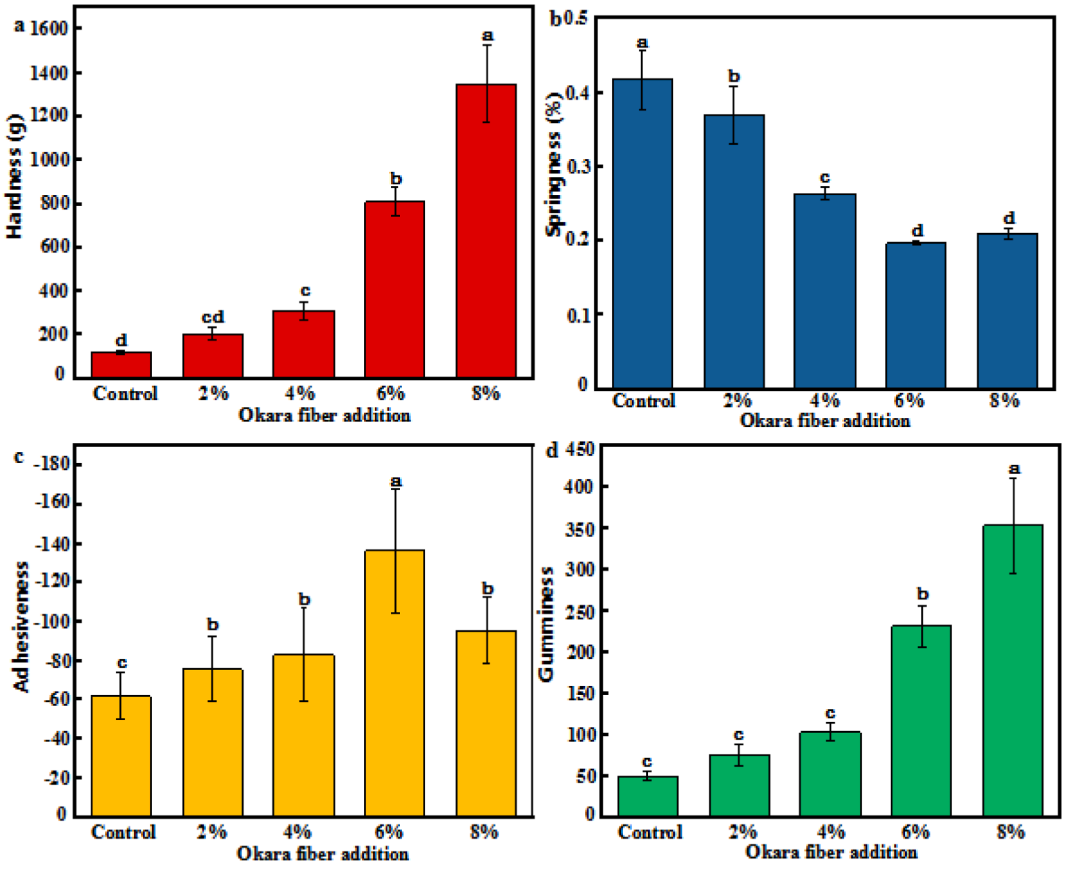

Fig. 6. The texture distribution analysis results of cookie dough with different content of okara fiber. a Hardness (g); b Springness (%); c Adhesiveness; d Gumminess.

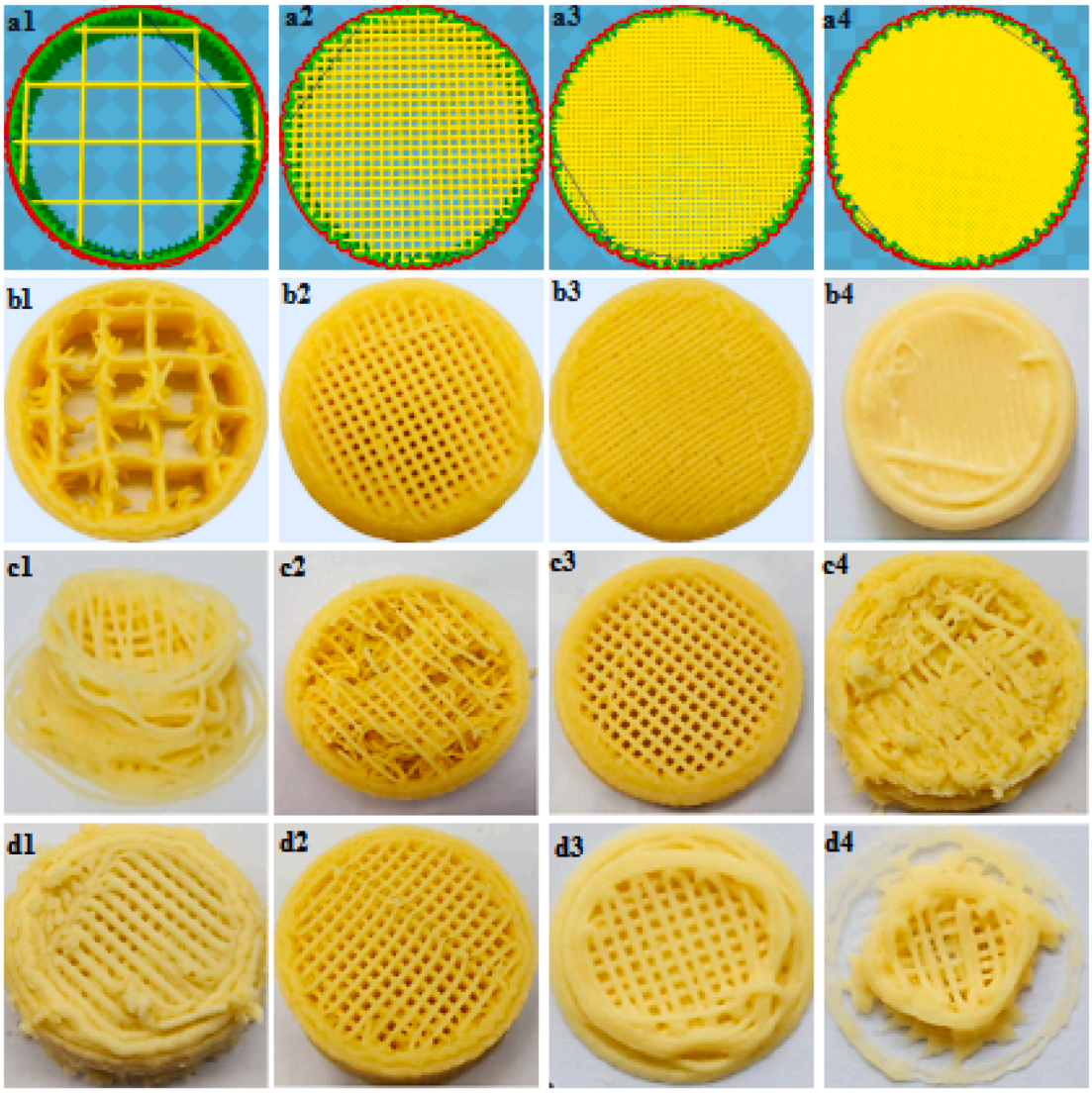

Fig. 7. (a) 3D drawings of models designed considering different filling rates (a1 = 10%, a2 = 30%, a3 = 50%, a4 = 70%) as well as (b) photos of cylindrical cookie, (c) nozzle diameters (c1 = 0.4 mm, c2 = 0.6 mm, c3 = 0.8 mm, c4 = 1 mm) and (d) printing speeds (d1 = 25 mm/s, d2 = 50 mm/s, d3 = 75 mm/s, d4 = 100 mm/s).

cross, parallel, and unsupported structures, and the results indicated that the 3D-printed chocolate with cross supporting structures was the most stable [51].

3.4.2. Optimization of nozzle diameter

The size of the nozzle diameter directly affects the precision and surface roughness of the printed product [52]. It is clear that the final quality of the printed product increases as the nozzle diameter decreases [30]. Fig. 7c shows the visual appearance of printed cylinders with different nozzle diameters (c1 = 0.4 mm, c2 = 0.6 mm, c3 = 0.8 mm, c4 = 1.0 mm). The cylinder printed with a nozzle diameter of 0.8 mm presents a higher resolution and the smoothest surface structure (Fig. 7c3). However, a larger nozzle diameter will lead to a relatively rough surface of the printed cylinder and poor printing quality. This is because the large amount of material extruded from the nozzle destroys the pre-adjusted shape of the model and results in poor print quality (Fig. 7c4). A smaller nozzle diameter will lead to high surface precision of the printing cylinder and longer printing time. However, under the condition of constant air pressure, the smaller the hole diameter, the greater the pressure the dough will experience when it is extruded from the nozzle. Therefore, during the printing process, the cookie dough cannot be stacked on the surface of the printing table in an orderly manner (Fig. 7c1). As the nozzle moves along a preset trajectory, although the cookie dough can be stacked one after another, the integrity of the internal structure is not guaranteed (Fig. 7c2). Therefore, a nozzle diameter of 0.8 mm is considered optimum.

3.4.3. Optimization of nozzle moving speed

The printing speed controls the rate at which the food material is deposited on the printing plate [53]. We also studied the effect of printing speed on the printing results to determine the dynamic working range of the 3D printer [30]. In general, the printing speed was closely related to the printing time and printing quality. Fig. 7d shows the influence of different printing speeds (d1 = 25 mm/s, d2 = 50 mm/s, d3 = 75 mm/s, and d4 = 100 mm/s) on the printing effect of the cylinder. With increasing printing speed, the surface structure of the cylinder becomes irregular or damaged by the nozzle, which further affects the texture of the printed product (Fig. 7d3 and d4). This is because the speed of ink extruding from the nozzle and the amount of ink cannot match the printing speed. Simultaneously, the rotation speed of the screw is also increased, thereby affecting the material deposition during the rapid printing process [54]. In addition, with the increase in the printing speed during the printing process, the length, width, and height of the printed product differ significantly from the original model. This

may lead to increased shear force and ink shear thinning, which further causes the printed sample structure to deviate from the model design [55]. With lower printing speeds, the surface structure of the ink becomes disordered, which may be caused by the ink flow instability (Fig. 7d1) [30]. Therefore, the best printing quality can be obtained at a printing speed of 50 mm/s (Fig. 7d2), and the surface of the cylindrical structure exhibits a clear outline.

3.5. Sensory evaluation of 3D-printed cookies

As already mentioned, in this study, the 3D-printed DF cookies were compared against three other commonly available types by evaluating their appearance, color, crispiness, taste, flavor, and overall quality based on a 5-point hedonic scale (Fig. 8). As can be seen, from the appearance perspective alone, the 3D-printed DF cookies score higher than the other three types. This can be attributed to the fact that the 3D-printing technology can be leveraged to design customized cookie shapes using CAD software, thereby achieving aesthetic diversity and greatly influencing panelist acceptance. Huebner et al. [56] have reported that the baking process involves the occurrence of the Maillard reaction, which occurs between the reducing sugars and amino acids present in the cookie raw material. These reactions produce compounds of higher molecular weight that influence the cookie color, flavor, and taste. Accordingly, the increased intensities of color, flavor, and taste observed in the 3D-printed cookies could be attributed to the occurrence of the Maillard reaction. Furthermore, DF structure contains a large number of hydrophilic groups, thereby demonstrating strong hydration characteristics [57]. The existence of hydration properties of DF in the cookie dough tends to affect the Maillard reaction such that the color, flavor, and taste of cookies containing DF are of slightly lower intensity compared to those of fiber-free cookies. The crispiness is an important factor influencing cookie acceptability [58]. In this study, the 3D-printed DF cookies beat the competition in the crispiness score. The fat content in cookies contributes to their crispiness. A gluten network is formed when the flour interacts with water during dough preparation. This gluten formation causes the dough to become tough, and therefore, it is undesirable during cookie preparation. Gluten formation can be prevented by increasing the fat content in the cookie formulation. The said fat coats the flour surface and isolates the starch granules and proteins, thereby interrupting the starch structure and protein integrity and facilitating the preparation of tender, crisp cookies [59]. It can be stated that the modified IDF demonstrates superior hydration properties, which further enhances the cookie crispiness [57]. In terms of overall quality, the 3D-printed cookies score higher compared to the cookie types. This implies that compared to the competition, the cookies prepared in this study via 3D printing and containing the modified okara fiber are more acceptable to the panelists.

4. Conclusions

In this study, ultrasound and high-speed shear were used to modify okara fibers. SEM, XRD, FT-IR, and DSC techniques were used to analyze such physical attributes of okara fiber as color, particle size, zeta potential, SC, WHC, and OHC. The results obtained in this study reveal that the okara fiber modified using the 500 W–15,000 rpm combination demonstrated the highest SC, WHC, and OHC values. In addition, the rheological properties of okara fiber were investigated, and TPA tests were performed by adding the modified okara fiber to cookie dough. The results reveal that when the okara-fiber concentration in dough equals 6%, the dough exhibited optimum adhesiveness and printability. Through optimization of the printing parameters, the best filling rate, nozzle diameter, and printing speed were determined as 30%, 0.8 mm, and 50 mm/s, respectively. Subsequently, the 3D-printed cookies were compared against those commonly available in the market via sensory evaluation. The results reveal the 3D-printed cookies to be more acceptable to the tasting panel. Therefore, it can be concluded that the addition of the modified okara fiber to cookie dough not only improves the latter's utilization rate but also increases the DF content in the cookies, thereby alleviating the occurrence of obesity in modern population. In addition, the introduction of 3D printing technology to food processing facilitates the diversification of cookie shapes.

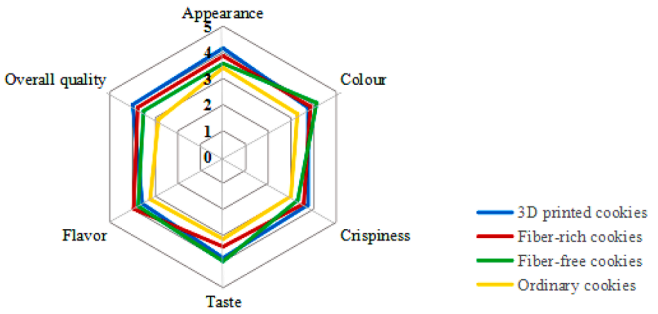

Fig. 8. Sensory evaluation of different cookie types.

CRediT authorship contribution statement

Yaowen Liu: Writing - original draft, Methodology. **Shengkui Yi:** Writing - original draft, Data curation. **Tingting Ye:** Visualization. **Ying Leng:** Data curation. **Md Alomgir Hossen:** Conceptualization. **Dur E. Sameen:** Conceptualization. **Jianwu Dai:** Software. **Suqing Li:** Conceptualization. **Wen Qin:** Writing - review & editing.

Declaration of Competing Interest

The authors declare that they have no known competing financial interests or personal relationships that could have appeared to influence the work reported in this paper.

Acknowledgments

This work was supported by National Natural Science Foundation of China (51703147), Sichuan Science and Technology Program (2019YFN0174, 2020JDRC0111, 2020YFN0149, and 2021JDRC0030).

References

[1] G. Fayaz, S. Plazzotta, S. Calligaris, L. Manzocco, M.C. Nicoli, Impact of high pressure homogenization on physical properties, extraction yield and biopolymer structure of soybean okara, LWT-Food Sci. Technol. 113 (2019), 108324, https://doi.org/10.1016/j.lwt.2019.108324.

[2] L. Jankowiak, O. Trifunovic, R.M. Boom, A.J.V.D. Goot, The potential of crude okara for isoflavone production, J. Food Eng. 124 (2014) 166–172, https://doi.org/10.1016/j.jfoodeng.2013.10.011.

[3] D.R. Lin, X.M. Long, Y.C. Huang, Y.M. Yang, Z.J. Wu, H. Chen, Q. Zhang, D.T. Wu, W. Qin, Z.C. Tu, Effects of microbial fermentation and microwave treatment on the composition, structural characteristics, and functional properties of modified okara dietary fiber, LWT-Food Sci. Technol. 123 (2020), 109059, https://doi.org/10.1016/j.lwt.2020.109059.

[4] N. Aravind, M. Sissons, N. Egan, C. Fellows, Effect of insoluble dietary fibre addition on technological, sensory, and structural properties of durum wheat spaghetti, Food Chem. 130 (2) (2012) 299–309, https://doi.org/10.1016/j.foodchem.2011.07.042.

[5] B. Li, W. Yang, Y.Y. Nie, F.F. Kang, H.D. Goff, S.W. Cui, Effect of steam explosion on dietary fiber, polysaccharide, protein and physicochemical properties of okara, Food Hydrocoll. 194 (2019) 48–56, https://doi.org/10.1016/j.foodhyd.2019.02.042.

[6] Y.J. Cai, L.H. Huang, B.F. Chen, J.Q. Su, X.J. Zhao, M.M. Zhao, Q.Z. Zhao, P.V. D. Meeren, Effect of homogenization associated with alkaline treatment on the structural, physicochemical, and emulsifying properties of insoluble soybean fiber (ISF), Food Hydrocoll. 113 (2021), 106516, https://doi.org/10.1016/j.foodhyd.2020.106516.

[7] C.L. Wu, F. Teng, D.J.M. Clements, S. Zhang, Y. Li, Z.J. Wang, Effect of cavitation jet processing on the physicochemical properties and structural characteristics of okara dietary fiber, Food Res. Int. 134 (2020), 109251, https://doi.org/10.1016/j.foodres.2020.109251.

[8] X.J. Wang, Y.Y. Zhang, Y.B. Li, H.S. Yu, Y.H. Wang, C.H. Piao, Insoluble dietary fibre from okara (soybean residue) modified by yeast Kluyveromyces marxianus,

LWT-Food Sci. Technol. 134 (2020), 110252, https://doi.org/10.1016/j.lwt.2020.110252.
[9] I. Ullah, T. Yin, S.B. Xiong, J. Zhang, Z. Din, M.L. Zhang, Structural characteristics and physicochemical properties of okara (soybean residue) insoluble dietary fiber modified by high-energy wet media milling, LWT-Food Sci. Technol. 82 (2017) 15–22, https://doi.org/10.1016/j.lwt.2017.04.014.
[10] B.Y. Yoshida, S.H. Prudencio, Physical, chemical, and technofunctional properties of okara modified by a carbohydrase mixture, LWT-Food Sci. Technol. 134 (2020), 110141, https://doi.org/10.1016/j.lwt.2020.110141.
[11] M. Singla, N. Sit, Application of Ultrasound in Combination with Other Technologies in Food Processing: A Review, Ultrason. Sonochem. 73 (2021) 105506, https://doi.org/10.1016/j.ultsonch.2021.105506.
[12] X.J. Fan, H.D. Chang, Y.N. Lin, X.M. Zhao, A. Zhang, S. Li, Z. Feng, X. Chen, Effects of ultrasound-assisted enzyme hydrolysis on the microstructure and physicochemical properties of okara fibers, Ultrason. Sonochem. 69 (2020), 105247, https://doi.org/10.1016/j.ultsonch.2020.105247.
[13] W.M. Zhang, G.L. Zeng, Y.G. Pan, W.X. Chen, W.Y. Huang, H.M. Chen, Y.S. Li, Properties of soluble dietary fiber-polysaccharide from papaya peel obtained through alkaline or ultrasound-assisted alkaline extraction, Carbohydr. Polym. 172 (2017) 102–112, https://doi.org/10.1016/j.carbpol.2017.05.030.
[14] M. Moczkowska, S. Karp, Y. Niu, M.A. Kurek, Enzymatic, enzymatic-ultrasonic and alkaline extraction of soluble dietary fibre from flaxseed – A physicochemical approach, Food Hydrocoll. 90 (2019) 105–112, https://doi.org/10.1016/j.foodhyd.2018.12.018.
[15] K.C. Martinez-Solano, N.A. Garcia-Carrera, V. Tejada-Ortigoza, T. García-Cayuela, L.E. Garcia-Amezquita, Ultrasound Application for the Extraction and Modification of Fiber-Rich By-Products, Food Eng. Rev. 185 (2020) 1–20, https://doi.org/10.1007/s12393-020-09269-2.
[16] C.Z. Wang, L. Li, X. Sun, W. Qin, D.T. Wu, B. Hu, D. Raheem, W.Y. Yang, H. M. Dong, T. Vasanthan, Q, Zhang, High-speed shearing of soybean flour suspension disintegrates the component cell layers and modifies the hydration properties of okara fibers, LWT-Food Sci. Technol. 116 (2019), 108505, https://doi.org/10.1016/j.lwt.2019.108505.
[17] J.Y. Huang, J.S. Liao, J.R. Qi, W.X. Jiang, X.Q. Yang, Structural and physicochemical properties of pectin-rich dietary fiber prepared from citrus peel, Food Hydrocoll. 110 (2021), 106140, https://doi.org/10.1016/j.foodhyd.2020.106140.
[18] C.G. Jr, I.C.O. Neves, L.T. Lim, B.M. Bohrer, R.C. Rodrigues, C. Prentice, Characterization of dietary fiber from residual cellulose sausage casings using a combination of enzymatic treatment and high-speed homogenization, Food Hydrocoll. 100 (2020), 105398, https://doi.org/10.1016/j.foodhyd.2019.105398.
[19] W. Dong, D. Wang, R. Hu, Y. Long, L. Lv, Chemical composition, structural and functional properties of soluble dietary fiber obtained from coffee peel using different extraction methods, Food Res. Int. 136 (2020) 109497, https://doi.org/10.1016/j.foodres.2020.109497.
[20] J. Park, I. Choi, Y. Kim, Y, Kim, Cookies formulated from fresh okara using starch, soy flour and hydroxypropyl methylcellulose have high quality and nutritional value, LWT-Food Sci. Technol. 63 (1) (2015) 660–666, https://doi.org/10.1016/j.lwt.2015.03.110.
[21] D.P.S. Lee, A.X. Gan, J.E. Kim, Incorporation of biovalorised okara in biscuits: Improvements of nutritional, antioxidant, physical, and sensory properties, LWT-Food Sci. Technol. 134 (2020), 109902, https://doi.org/10.1016/j.lwt.2020.109902.
[22] K. Kahraman, E. Aktas-Akyildiz, S. Ozturk, H. Koksel, Effect of different resistant starch sources and wheat bran on dietary fibre content and in vitro glycaemic index values of cookies, J. Cereal Sci. 90 (2019), 102851, https://doi.org/10.1016/j.jcs.2019.102851.
[23] Y.A. Sun, M. Zhanga, H.Z. Chen, LF-NMR intelligent evaluation of rheology and printability for 3D printing of cookie dough pretreated by microwave, LWT-Food Sci. Technol. 132 (2020), 109752, https://doi.org/10.1016/j.lwt.2020.109752.
[24] Z. Liu, B. Bhandari, S. Prakash, S. Mantihal, M. Zhang, M, Zhang, Linking rheology and printability of a multicomponent gel system of carrageenan-xanthan-starch in extrusion based additive manufacturing, Food Hydrocoll. 87 (2019) 413–424, https://doi.org/10.1016/j.foodhyd.2018.08.026.
[25] Y.L. Yang, E. Guan, T.J. Zhang, M.M. Li, K. Bian, Influence of water addition methods on water mobility characterization and rheological properties of wheat flour dough, J. Cereal Sci. 89 (2019), 102791, https://doi.org/10.1016/j.jcs.2019.102791.
[26] E. Pulatsu, J.W. Su, S.M. Kenderes, J. Lin, B. Vardhanabhuti, M.S. Lin, Effects of ingredients and pre-heating on the printing quality and dimensional stability in 3D printing of cookie dough, J. Food Eng. 294 (2021), 110412, https://doi.org/10.1016/j.jfoodeng.2020.110412.
[27] I. Ullah, T. Yin, S.B. Xiong, Q.L. Huang, Z. Din, J. Zhang, A.B. Javaid, Effects of thermal pre-treatment on physicochemical properties of nano-sized okara (soybean residue) insoluble dietary fiber prepared by wet media milling, J. Food Eng. 237 (2018) 18–26, https://doi.org/10.1016/j.jfoodeng.2018.05.017.
[28] H.W. Kim, J. Lee, S.M. Park, J.H. Lee, M.H. Nguyen, H.J. Park, Effect of hydrocolloid addition on dimensional stability in post-processing of 3D printable cookie dough, LWT-Food Sci. Technol. 101 (2019) 69–75, https://doi.org/10.1016/j.lwt.2018.11.019.
[29] X. Hua, S. Xu, M.M. Wang, Y. Chen, H. Yang, R.J. Yang, Effects of high-speed homogenization and high-pressure homogenization on structure of tomato residue fibers, Food Chen. 232 (2017) 443–449, https://doi.org/10.1016/j.foodchem.2017.04.003.
[30] L. Wang, M. Zhang, B. Bhandari, C.H. Yang, Investigation on fish surimi gel as promising food material for 3D printing, J. Food Eng. 220 (2018) 101–108, https://doi.org/10.1016/j.jfoodeng.2017.02.029.
[31] Y.W. Liu, Y. Yu, C.S. Liu, J.M. Regenstein, X.M. Liu, P. Zhou, Rheological and mechanical behavior of milk protein composite gel for extrusion-based 3D food printing, LWT-Food Sci. Technol. 102 (2019) 338–346, https://doi.org/10.1016/j.lwt.2018.12.053.
[32] P. Li, G. Wu, D. Yang, H. Zhang, X.G. Qi, Q.Z. Jin, X.G. Wang, Analysis of quality and microstructure of freshly potato strips fried with different oils, LWT-Food Sci. Technol. 133 (2020), 110038, https://doi.org/10.1016/j.lwt.2020.110038.
[33] M.M. Ma, T.H. Mu, Effects of extraction methods and particle size distribution on the structural, physicochemical, and functional properties of dietary fiber from deoiled cumin, Food Chem. 194 (2016) 237–246, https://doi.org/10.1016/j.foodchem.2015.07.095.
[34] Y. Wen, M. Niu, B.J. Zhang, S.M. Zhao, S.B. Xiong, Structural characteristics and functional properties of rice bran dietary fiber modified by enzymatic and enzyme-micronization treatments, LWT-Food Sci. Technol. 75 (2017) 344–351, https://doi.org/10.1016/j.lwt.2016.09.012.
[35] J. Velásquez-Cock, P. Gañán, P. Posada, C. Castro, A. Serpa, C. Gómez H., J.-L. Putaux, R. Zuluaga, R, Zuluaga, Influence of combined mechanical treatments on the morphology and structure of cellulose nanofibrils: Thermal and mechanical properties of the resulting films, Ind. Crops. Prod. 85 (2016) 1–10, https://doi.org/10.1016/j.indcrop.2016.02.036.
[36] T. Yang, H.L. Yan, C.H. Tang, Wet media planetary ball milling remarkably improves functional and cholesterol-binding properties of okara, Food Hydrocoll. 111 (2021), 106386, https://doi.org/10.1016/j.foodhyd.2020.106386.
[37] B.F. Chen, Y.G. Cai, T.X. Liu, L.H. Huang, X.L. Deng, Q.Z. Zhao, M.M. Zhao, Improvements in physicochemical and emulsifying properties of insoluble soybean fiber by physical-chemical treatments, Food Hydrocoll. 93 (2019) 167–175, https://doi.org/10.1016/j.foodhyd.2019.01.058.
[38] D. Mudgil, S. Barak, B.S. Khatkar, X-ray diffraction, IR spectroscopy and thermal characterization of partially hydrolyzed guar gum, Int. J. Biol. Macromol. 50 (4) (2012) 1035–1039, https://doi.org/10.1016/j.ijbiomac.2012.02.031.
[39] C.L. Wu, D.J. Mcclements, M.Y. He, L. Zheng, Y. Li, T. Tian, F. Teng, Y. Li, Preparation and characterization of okara nanocellulose fabricated using sonication or high-pressure homogenization treatments, Carbohydr. Polym. 255 (2021), 117364, https://doi.org/10.1016/j.carbpol.2020.117364.
[40] J. Perez-Jimenez, M.E. Diaz-Rubio, M. Mesias, F.J. Morales, F. Saura-Calixto, Evidence for the formation of maillardized insoluble dietary fiber in bread: A specific kind of dietary fiber in thermally processed food, Food Res. Int. 55 (2014) 391–396, https://doi.org/10.1016/j.foodres.2013.11.031.
[41] S.R. Falsafi, Y. Maghsoudlou, H. Rostamabadi, M.M. Rostamabadi, H. Hamedi, S.M. H. Hosseinie, Preparation of physically modified oat starch with different sonication treatments, Food Hydrocoll. 89 (2019) 311–320, https://doi.org/10.1016/j.foodhyd.2018.10.046.
[42] X.J. Fan, S. Li, A. Zhang, H.D. Chang, X.M. Zhao, Y.N. Lin, Z. Feng, Mechanism of change of the physicochemical characteristics, gelation process, water state, and microstructure of okara tofu analogues induced by high-intensity ultrasound treatment, Food Hydrocoll. 111 (2021) 106241, https://doi.org/10.1016/j.foodhyd.2020.106241.
[43] Z.B. Liu, M. Zhang, B. Bhandari, Y.C. Wang, 3D printing: Printing precision and application in food sector, Trends Food Sci. Tech. 69 (2017) 83–94, https://doi.org/10.1016/j.tifs.2017.08.018.
[44] D.P. Bolhuis, C.G. Forde, Application of food texture to moderate oral processing behaviors and energy intake, Trends Food Sci. Tech. 106 (2020) 445–456, https://doi.org/10.1016/j.tifs.2020.10.021.
[45] M. Lille, A. Nurmela, E. Nordlund, S. Metsa-Kortelainen, N. Sozer, Applicability of protein and fiber-rich food materials in extrusion-based 3D printing, J. Food Eng. 220 (2018) 20–27, https://doi.org/10.1016/j.jfoodeng.2017.04.034.
[46] Z.B. Liu, M. Zhang, B. Bhandari, C.H. Yang, Impact of rheological properties of mashed potatoes on 3D printing, J. Food Eng. 220 (2018) 76–82, https://doi.org/10.1016/j.jfoodeng.2017.04.017.
[47] William J. Costakis, Lisa M. Rueschhoff, Andres I. Diaz-Cano, Jeffrey P. Youngblood, Rodney W. Trice, Additive manufacturing of boron carbide via continuous filament direct ink writing of aqueous ceramic suspensions, J. Eur. Ceram. Soc. 36 (14) (2016) 3249–3256, https://doi.org/10.1016/j.jeurceramsoc.2016.06.002.
[48] D. Cando, A.J. Borderías, H.M. Moreno, Combined effect of aminoacids and microbial transglutaminase on gelation of low salt surimi content under high pressure processing, Innov. Food Sci. Emerg. Technol. 36 (2016) 10–17, https://doi.org/10.1016/j.ifset.2016.05.010.
[49] Z.B. Liu, B. Bhandari, S. Prakash, M. Zhang, Creation of internal structure of mashed potato construct by 3D printing and its textural properties, Food Res. Int. 111 (2018) 534–543, https://doi.org/10.1016/j.foodres.2018.05.075.
[50] Y.W. Liu, X. Liang, A. Saeed, W.J. Lan, W. Qin, Properties of 3D printed dough and optimization of printing parameters, Innov. Food Sci. Emerg. Technol. 54 (2019) 9–18, https://doi.org/10.1016/j.ifset.2019.03.008.
[51] S. Mantihal, S. Prakash, F.C. Godoi, B. Bhandari, Optimization of chocolate 3D printing by correlating thermal and flow properties with 3D structure modeling, Innov. Food Sci. Emerg. Technol. 44 (2017) 21–29, https://doi.org/10.1016/j.ifset.2017.09.012.
[52] F. Vogeler, W. Verheecke, A. Voet, H. Valkenaers, An initial study of aerosol jet® printed interconnections on extrusion-based 3D-printed substrates, J. Mech. Eng. 59 (11) (2013) 689–696, https://doi.org/10.5545/sv-jme10.5545/sv-jme10.5545/sv-jme.2013.999.

[53] C. Severini, D. Azzollini, M. Albenzio, A. Derossi, On printability, quality and nutritional properties of 3D printed cereal based snacks enriched with edible insects, Food Res. Int. 106 (2018) 666–676, https://doi.org/10.1016/j.foodres.2018.01.034.

[54] A. Derossi, M. Paolillo, R. Caporizzi, C. Severini, Extending the 3D food printing tests at high speed. Material deposition and effect of non-printing movements on the final quality of printed structures, J. Food Eng. 275 (2020), 109865, https://doi.org/10.1016/j.jfoodeng.2019.109865.

[55] Y.M. Shi, M. Zhang, B. Bhandari, Effect of addition of beeswax based on 3D printing of potato starch-protein system, Food Struct. 27 (2021), 100176, https://doi.org/10.1016/j.foostr.2021.100176.

[56] J. Huebner, R.L. Wehling, A. Parkhurst, R.W. Hutkins, Effect of processing conditions on the prebiotic activity of commercial prebiotics, Int. Dairy J. 18 (3) (2008) 287–293, https://doi.org/10.1016/j.idairyj.2007.08.013.

[57] M. Föste, C. Verheyen, M. Jekle, T. Becker, Fibres of milling and fruit processing by-products in gluten-free bread making: A review of hydration properties, dough formation and quality-improving strategies, Food Chem. 306 (2020), 125451, https://doi.org/10.1016/j.foodchem.2019.125451.

[58] J. Park, I. Choi, Y. Kim, Cookies formulated from fresh okara using starch, soy flour and hydroxypropyl methylcellulose have high quality and nutritional value, LWT – Food Sci. Technol. 63 (1) (2015) 660–666, https://doi.org/10.1016/j.lwt.2015.03.110.

[59] M.M. Ekin, N. Kutlu, R. Meral, Z. Ceylan, İ. Cavidoglu, A novel nanotechnological strategy for obtaining fat-reduced cookies in bakery industry: Revealing of sensory, physical properties, and fatty acid profile of cookies prepared with oil-based nanoemulsions, Food Biosci. 42 (2021), 101184, https://doi.org/10.1016/j.fbio.2021.101184.